RSC Advances

ROYAL SOCIETY OF CHEMISTRY

www.rsc.org/advances

Table of Contents

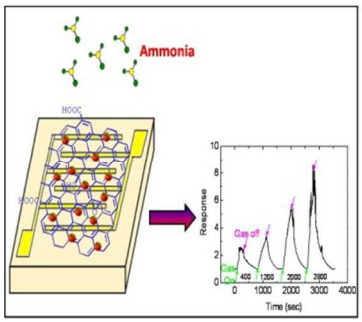

RGO–SnO_2 based highly selective and ultra-sensitive ammonia detector at room temperature.

Enhanced Ammonia Sensing at Room Temperature with Reduced Graphene Oxide/ Tin Oxide Hybrid Film

Ruma Ghosh[a], *Arpan Kumar Nayak*[b], *Sumita Santra*[c], *Debabrata Pradhan*[b], *Prasanta Kumar Guha*[a]*

[a]Department of Electronics & Electrical Communication Engineering, Indian Institute of Technology, Kharagpur-721302, India

[b] Centre of Material Science, Indian Institute of Technology, Kharagpur-721302, India

[c]Department of Physics, Indian Institute of Technology, Kharagpur-721302, India

Abstract

Sensitive and selective detection of ammonia at room temperature is required for proper environmental monitoring and also to avoid any health hazards in the industrial areas. The excellent electrical properties of reduced graphene oxide (RGO) and sensing capabilities of SnO_2 were combined to achieve enhanced ammonia sensitivity. RGO−SnO_2 films were synthesized hydrothermally as well as prepared by the mixing different amounts of hydrothermally synthesized SnO_2 nanoparticles to graphene oxide (GO). It was observed that the response of the hybrid sensing layer was much better than intrinsic RGO or SnO_2. But the best performance was observed in 10:8 (RGO−SnO_2) sample. The sample was exposed to nine different concentrations

of ammonia in presence of 20% RH at room temperature. The response of the sensor varied from 1.4 times (25 ppm) to 22 times (2800 ppm) with quick recovery after purging with air. The composite formation was verified by characterizing the samples using field emission scanning electron microscopy (FESEM), X-ray diffractometer (XRD), X-ray photoelectron spectroscopy (XPS) and high resolution transmission electron microscopy (HRTEM). The results and their significance have been discussed in details.

1. Introduction

Ammonia is a toxic pollutant which occurs naturally in environment through human wastes and industries.[1] It has a sharp and pungent odor but we can smell it only if the concentration of ammonia is more than 50 ppm (parts per million).[2] So, it is quite natural to get exposed to lower levels of ammonia in day-to-day lives without even knowing. Ammonia can cause severe affects on human body like irritation in eyes, throat, skin and respiratory systems when exposed to concentration greater than 35 ppm for even 15 minutes.[3] So, it is necessary to develop highly sensitive and selective ammonia sensor that can detect low concentrations of ammonia.

Tin dioxide (SnO_2) is an n-type semiconducting material. It is highly sensitive towards different chemical analytes.[4-6] Different morphologies of SnO_2 nanostructures and its composite have already been employed as ammonia sensors in the past few years.[7] But like other metal oxides, SnO_2 also suffers from two major drawbacks− first is high temperature operability, i.e. it can sense gases only at elevated temperature (200−500ºC) which increases the power consumption as well as limits its feasibility as sensor in conditions where high temperature operations are not allowed.[8] The second drawback is poor selectivity, i.e. tin oxide shows similar response towards different gases and thereby demonstrates no specificity towards any particular gas.[9]

In this regards, graphene and reduced graphene oxide (RGO) gain advantage. Graphene is a 2-D carbon nanomaterial with high aspect ratio and excellent electronic properties which facilitate sensing gases at room temperature.[10] However graphene in its pure form is not ideal for gas detection, because it is devoid of any functional groups and defect sites which play vital role in gas sensing. Also, graphene can usually be synthesized using sophisticated and expensive techniques like chemical vapor deposition (CVD), epitaxial method etc.,[11] one of the cheapest technique to synthesize graphene is through mechanical exfoliation but that too suffers with scalability issue.[12] RGO on the other hand can be synthesized chemically, which is usually a low cost technique and also RGO contains functional groups and defect sites which act as active regions for the gas molecules to get attached.[13] But the response of RGO towards gases is not as high as that of metal oxides.

Inspired by the outstanding properties of RGO and SnO_2 (RGO can sense gases at room temperature and SnO_2 gives large response), here we have developed RGO−SnO_2 hybrid samples for ammonia sensing. RGO, intrinsically a p-type material, was synthesized by reducing graphene oxide (GO) thermally. The n-type SnO_2 nanoparticles were synthesized using hydrothermal technique. The RGO−SnO_2 hybrid material was prepared in two ways which has been discussed in the experimental section. The sensor was featured with very large response (larger than RGO or SnO_2 response towards ammonia), good selectivity, fast response and recovery even at room temperature. The enhanced sensing behavior of the hybrid film is due to the combined nature of p-type and n-type sensing material. The response of the sensor was carried out in presence of ammonia (25−2800ppm) and different VOCs. The sensing results and their mechanism have been explained in details.

2. Experimental Section

2.1 Material synthesis

2.1.1 **Chemicals –** Fine graphite powder was purchased from Loba Chemie Pvt. Ltd., India and Stannous chloride hydrate [$SnCl_2 \cdot 2H_2O$], from Sisco Research Laboratories (SRL), India. All the other chemicals were purchased from Merck, India. All the above reagents were analytical grade and used without further purification.

2.1.2 **GO/RGO Synthesis –** GO was synthesized using modified Hummers' method as has been reported earlier.[14] Briefly, graphite powder was exfoliated using $NaNO_3$, H_2SO_4 and $KMnO_4$. After synthesizing GO, the solution was centrifuged at a speed of 5000 rpm to eliminate the visible particles. The hence, purified GO was reduced thermally by heating at 160ºC in air ambience for 30 minutes to obtain RGO.

2.1.3 **SnO_2 nanoparticle synthesis –** SnO_2 nanoparticles were synthesized by following procedure. First, 0.54g stannous chloride hydrate (0.06 M) was dissolved in 40 mL distilled water and the solution was stirred for 5 minutes. Then 1 mL of concentrated HCl was added to the above solution and stirred vigorously for 30 minutes prior to transfer it to a 50 mL Teflon-lined stainless steel autoclave. The autoclave was heated at 200°C for 12h and cooled naturally to room temperature. The powder product was collected by centrifuging. Finally, the as synthesized product was washed several times by water and ethanol and then calcined at 400°C for 2h.

2.1.4 **RGO–SnO_2 hybrid film preparation –** The hybrid sensing layer was prepared in two ways. (i) First, 40 mL of aqueous GO solution (2 mg/mL) was prepared by dispersion to which 0.54g stannous chloride hydrate was added and then 1 mL HCl was added and stirred before transferring to a stainless steel autoclave. Further steps were same as that of

SnO_2 nanoparticle synthesis. The GO got reduced during synthesis only as the solution was heated at 200ºC. (ii) The second method of hybrid film preparation was done by mixing GO and SnO_2 in different weight percentages. In this method, at first 100 mg GO was dispersed in 4 mL ethanol. The SnO_2 nanoparticles were then mixed to GO dispersed in ethanol by maintaining different weight ratios. Five such samples were prepared in which the wt% of GO and SnO_2 was varied as 10:3, 10:4, 10:5, 10:8 and 1:1. The GO–SnO_2 mixed samples were ultrasonicated for 30 minutes, so as to get uniform dispersion and also for proper mixing of GO and SnO_2 nanoparticles. The samples were then drop casted on Pt based interdigitated electrodes (Synkera Technologies, length and width of the electrode fingers being 2.54 mm and 100 µm respectively and having 100 µm space between two adjacent fingers), dried in air and then heated at 160ºC for 30 minutes to reduce the GO present in the hybrid sensing layer.

2.2 Material characterizations

The RGO–SnO_2 hybrid sensing layers were characterized using Zeiss Auriga Compact field emission scanning electron microscope (FESEM) to observe their morphologies as well as their composition. FEI TECNAI G2 high resolution transmission electron microscopy (HRTEM) was employed to observe the detailed microstructures of the hybrid sensing layers. The X-ray diffraction (XRD) pattern was observed using a Panalytical X'Pert Pro Diffractometer with a conventional X-ray tube (Cu Kα radiation). Also, in order to ensure proper reduction of GO to RGO, X-ray photoelectron spectroscopy (XPS) was done using PHI 5000 Versa Probe II.

2.3 Gas sensing

The gas sensing set-up was assembled in house. It consists of three mass flow controllers (MFCs) to control the flow rates of the gases, each MFC can allow maximum of 100 standard cubic centimeter per minute (sccm) of gas to flow through it; an airtight stainless steel chamber to probe the samples; and an Agilent 34972A LXI data acquisition (DAQ) card (which can record the resistance of the samples after every 5 sec) to interface the complete system with a computer.

3 Results and Discussion

3.1 Material characterizations

The SEM images of RGO, SnO_2 nanoparticles and the hybrid films are shown in Fig. 1

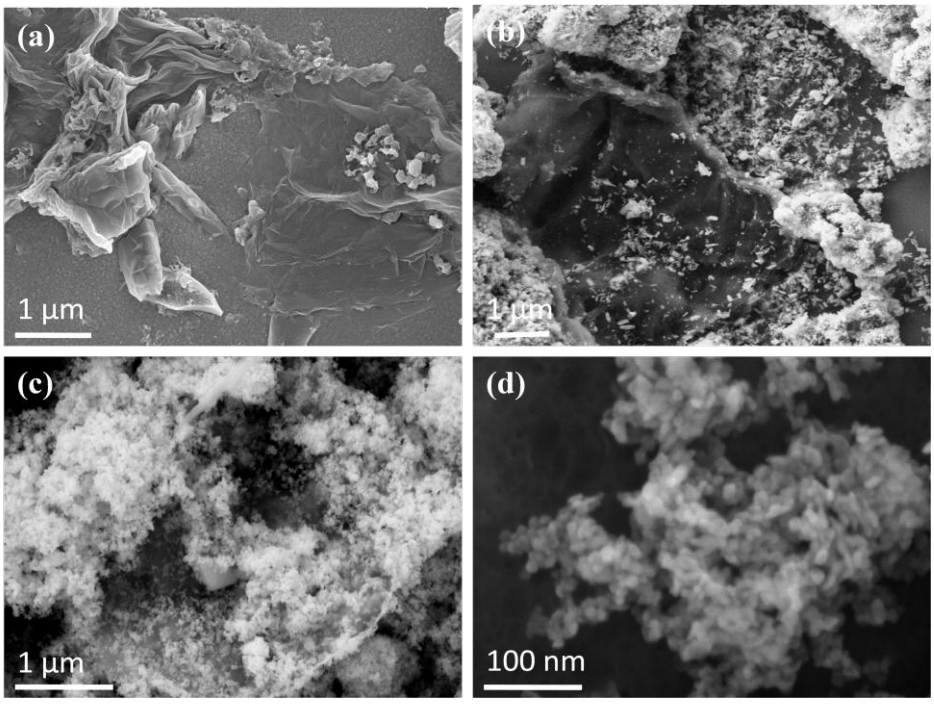

Fig. 1 SEM images of (a) thermally reduced GO (b, c) RGO–SnO_2 hybrid film prepared by mixing GO and SnO_2 (d) SnO_2 nanoparticles

The RGO film used to carry out ammonia sensing tests was multilayered as there are visible wrinkles in the SEM images of the RGO film as shown in Fig. 1(a). Fig. 1(b) shows the FESEM image of RGO–SnO_2 (10:3) hybrid film. The SnO_2 nanoparticles attached RGO flakes can be seen in the image. Also, it was observed that SnO_2 nanoparticles got agglomerated over the RGO flakes. Owing to their high surface energy, probably the SnO_2 nanoparticles got agglomerated while ultrasonicating the GO and metal oxide mixture in ethanol medium.1 The amount of SnO_2 particles got visibly increased when the proportion of SnO_2 was increased (ratio of RGO to SnO_2 was 10:8) as is shown in Fig. 1 (c). The FESEM image of 10:4, 10:5 and 1:1 RGO: SnO_2 samples are shown in Fig. S1 of Supporting Information. The FESEM of SnO_2 nanoparticles is shown in Fig. 1(d).

In order to ensure the composition of the hybrid samples synthesized both ways, energy dispersive X-ray spectroscopy (EDS) was carried out of all the samples. The EDS results of the samples are shown in Fig. 2.

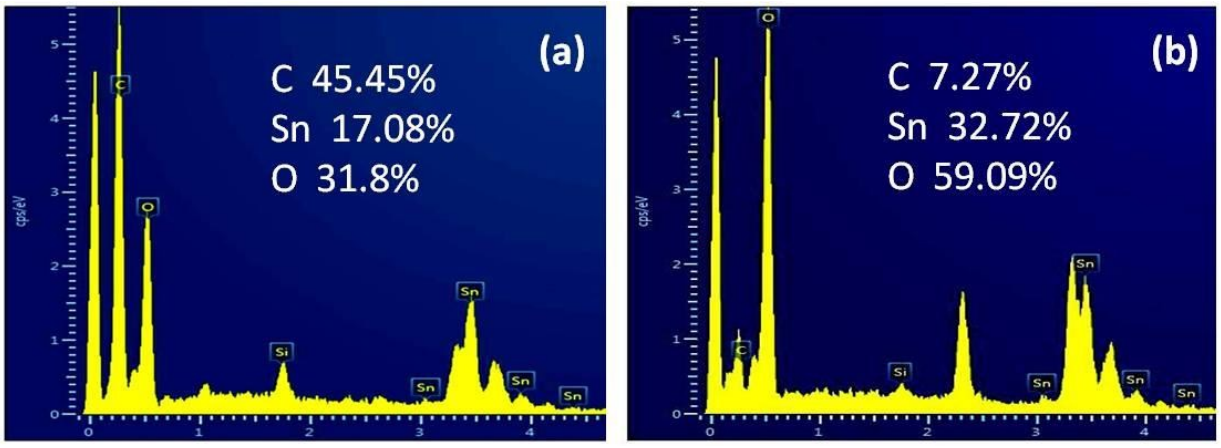

Fig. 2 EDS results of (a) 10:4 (RGO: SnO_2) hybrid samples (b) hydrothermally synthesized RGO−SnO_2 hybrid sample

The compositional analysis revealed the proportion of C, Sn and O present in the hybrid samples. Fig. 2 (a) shows the composition of RGO: SnO_2 hybrid sample prepared by mixing already synthesized GO and SnO_2 followed by thermal reduction. The EDS result of the hydrothermally synthesized hybrid sample is shown in Fig. 2 (b).

TEM was done to observe the crystalline nature and microstructural properties of the hybrid sensing materials prepared hydrothermally as well as by mixing GO and SnO_2 in different proportions. The TEM and HRTEM images of the samples are shown in Fig. 3.

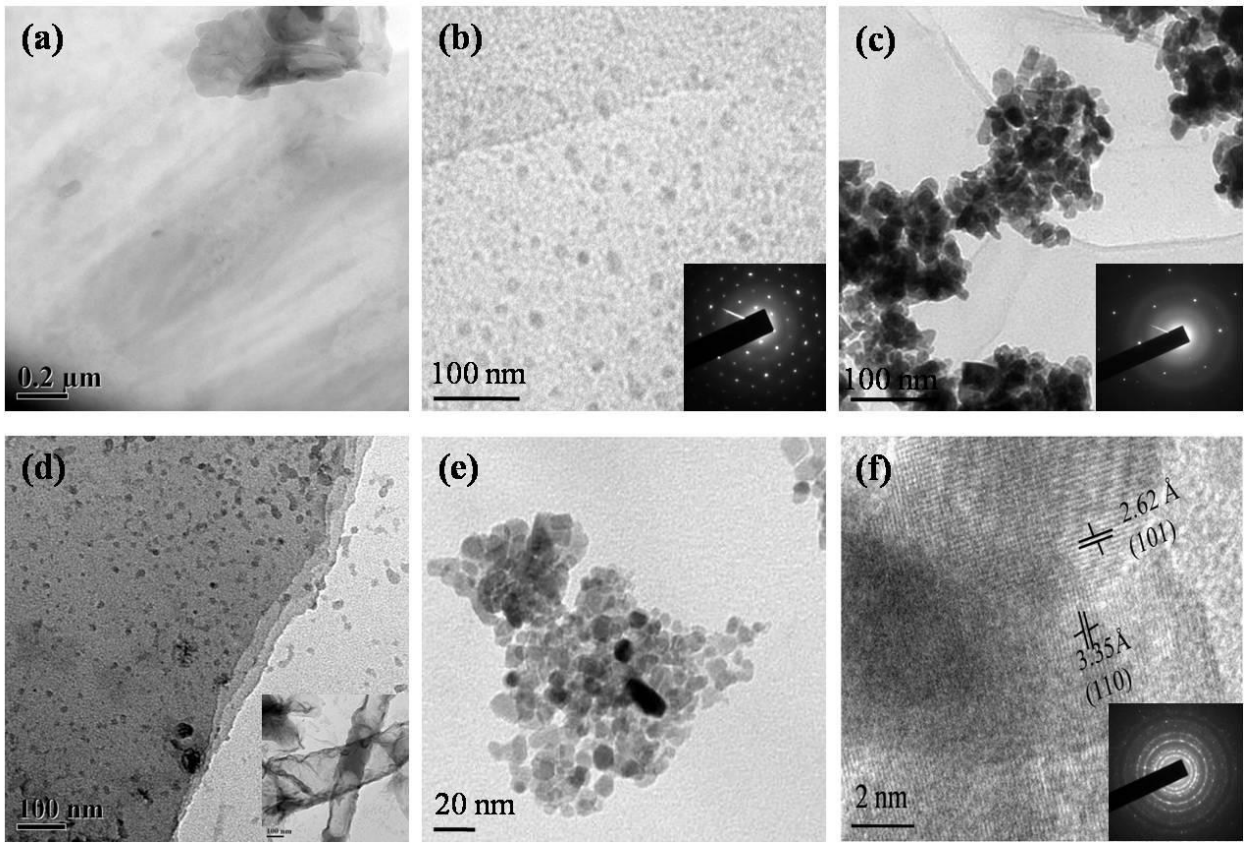

Fig. 3 TEM images of (a) thermally reduced GO (b) 10:3 (RGO: SnO_2) hybrid sample, inset shows the SAED pattern of the RGO (c) 10:8 (RGO: SnO_2) hybrid sample (d) hydrothermally synthesized RGO−SnO_2 sample, inset shows the folded and multilayered RGO (e) SnO_2

nanoparticles (f) HRTEM image of 10:8 (RGO: SnO_2), inset shows the SAED pattern of SnO_2 nanoparticles

The TEM image (Fig. 3 (a)) of thermally reduced GO appears to be transparent and few layered. Fig. 3 (b) shows the imprints of uniformly distributed SnO_2 nanoparticles (diameter ~10 nm) over RGO flake in 10:3 (RGO: SnO_2) hybrid sample. The inset shows the hexagonal rings of the RGO. Fig. 3 (c) demonstrates the presence of increased amount of SnO_2 nanoparticles in 10:8 (RGO: SnO_2) hybrid sample. The agglomeration of nanoparticles is clearly visible in the TEM image and also the same was observed in FESEM image. The inset of Fig. 3 (c) also shows the hexagonal ring of the C-atoms. Fig 3 (d) shows uniformly distributed SnO_2 nanoparticles over multilayered RGO flake in the hydrothermally synthesized RGO−SnO_2 hybrid sample. RGO in the hydrothermal sample attained different folded structure due to high temperature treatment. One such hollow tubular RGO structure found in the hydrothermally synthesized sample is shown in the inset of Fig. 3(d). The particle size of the SnO_2 nanoparticles were around 10 nm as can be seen in Fig. 3(e). Fig 3 (f) shows the HRTEM image of 10:8 (RGO: SnO_2) sample. It shows the presence of (101) and (110) SnO_2 planes in the hybrid sample which are perpendicular to each other. The result agrees well with the XRD data of SnO_2 nanoparticles as shown in Fig. 4. Also, the SAED pattern of the SnO_2 nanoparticles was found to be polycrystalline as is shown in the inset of Fig. 3(f)

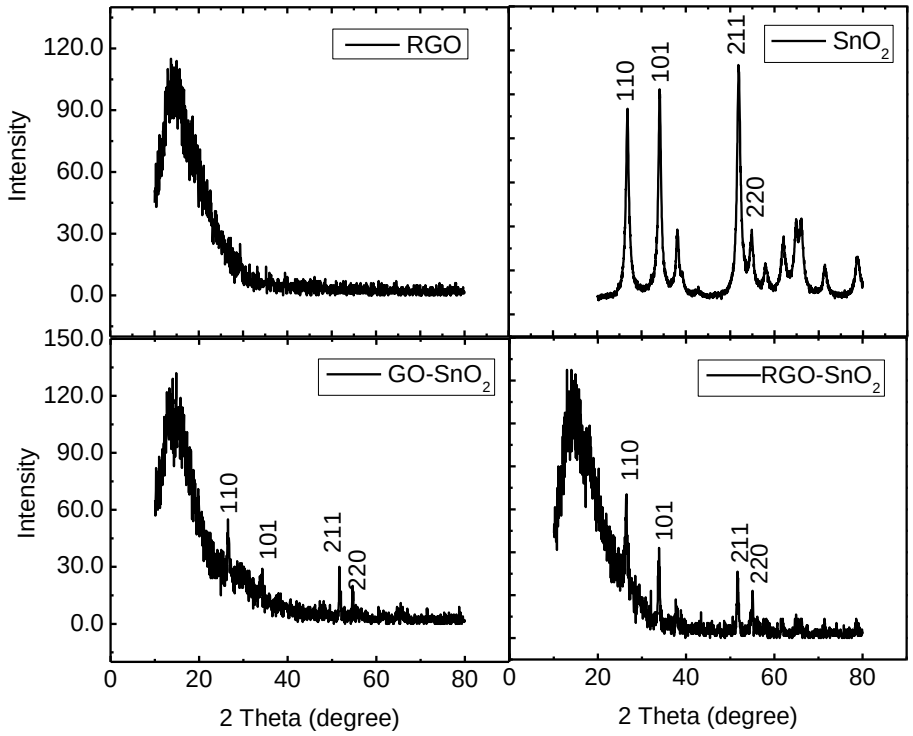

Fig. 4 XRD results of 30 minutes thermally reduced GO, SnO_2, GO–SnO_2, and RGO–SnO_2

A broad peak at around 15° was observed in the 30 minutes thermally reduced GO sample as is shown in Fig. 4. For SnO_2 nanoparticles, the sharp peaks were observed which signify its highly crystalline nature. Our observed SnO_2 XRD result matched well with the tetragonal structure of SnO_2 with lattice constant a = 4.7552, b = 4.7552 and, c = 3.1992 (JCPDS No. 01-077-0452). For the hybrid samples, the XRD of 10:8 (RGO: SnO_2) before and after reducing it thermally were carried out. Although no significant peak shifting corresponding to the reduction of GO was observed, but peaks of both RGO and SnO_2 nanoparticles are clearly visible in GO–SnO_2 and RGO–SnO_2 sample.

The elemental and compositional information of the hybrid samples were further investigated using XPS. The XPS results of the RGO–SnO_2 samples are shown in Fig. 5.

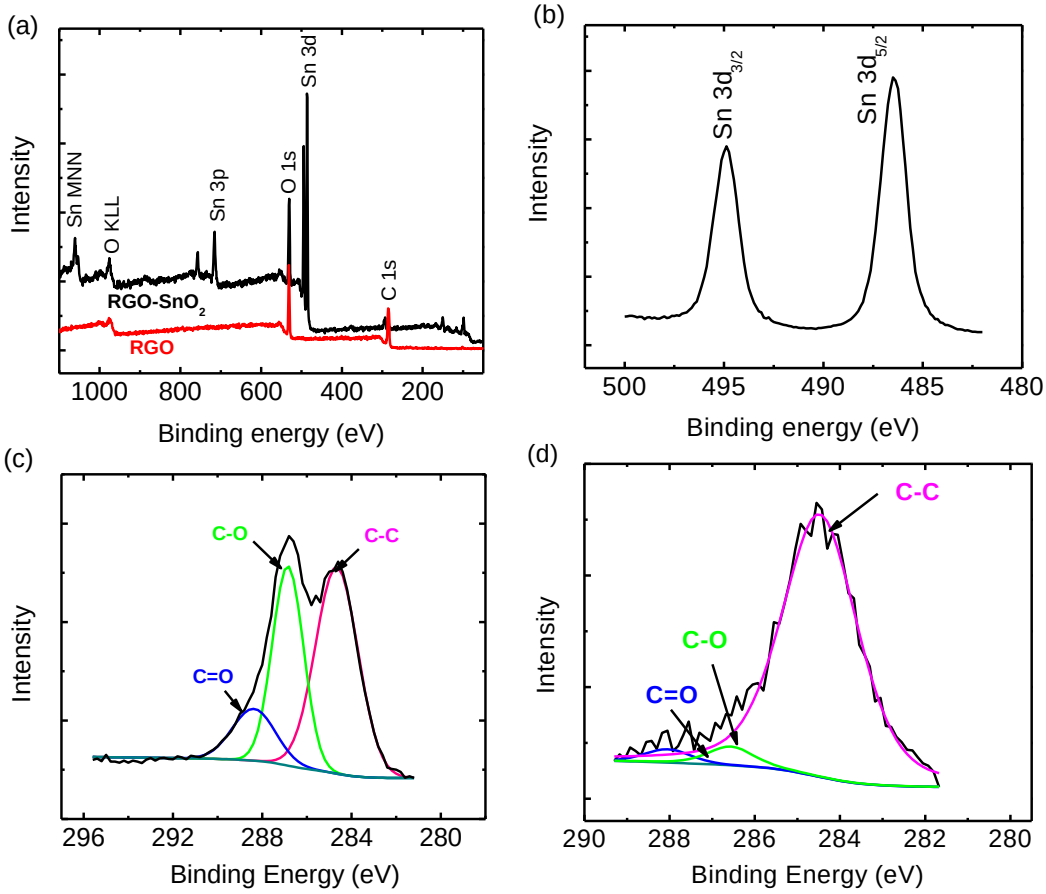

Fig. 5 XPS results of (a) comparative survey scan of RGO and RGO− SnO_2 (b) Sn 3d spectra in RGO− SnO_2 hybrid sample (c) C 1s peak of GO (d) C 1s peak of RGO− SnO_2 hybrid sample

The surface spectrum of RGO−SnO_2 sample (Fig. 5 (a)) clearly shows presence of carbon, oxygen and tin. No other peaks corresponding to the precursors of the samples (GO or SnO_2) were observed hence signifying that the samples were highly pure. Two Sn 3d peaks were observed at 486.4 and 494.8 eV which correspond to Sn $3d_{5/2}$ and Sn $3d_{3/2}$ respectively as shown in Fig. 5 (b).[15] These peaks are attributed to +4 oxidation states of Sn in RGO−SnO_2 hybrid

samples. The C 1s peak of GO can be de-convoluted into three peaks 284.5, 286.6 and 288.3 eV corresponding to C−C, C−O and C=O respectively.[16] The peak intensities corresponding C−O and C=O got reduced significantly after thermally reducing the RGO−SnO_2 sample as is evident from Fig. 5 (d), thereby signifying that the GO got properly reduced. One interesting observation that was made during the XPS characterization was that the intensities of the peaks corresponding to C−O and C=O in GO−SnO_2 were very less and were almost similar to that of 30 minutes reduced GO−SnO_2 sample. This signifies that the SnO_2 nanoparticles assisted in reduction of the GO. Similar results were observed in XRD also where no considerable peak shift was observed as shown in Fig. 4. But no measurable resistance could be measured at room temperature in the GO−SnO_2 samples unless those were thermally reduced for 30 minutes.

Gas sensing results

The sensors were developed on ceramic substrates. The substrates contain platinum interdigitated electrodes (IDEs) for measuring the resistance of the sensing layer. The hybrid samples were drop coated on these IDEs. The conductivities of the RGO, RGO–SnO_2 and SnO_2 samples are mentioned in the Supporting Information. The optical image of the sensor device is shown in Fig. 6 (a) and Fig. 6 (b) shows the schematic of the hence fabricated RGO–SnO_2 based sensor device.

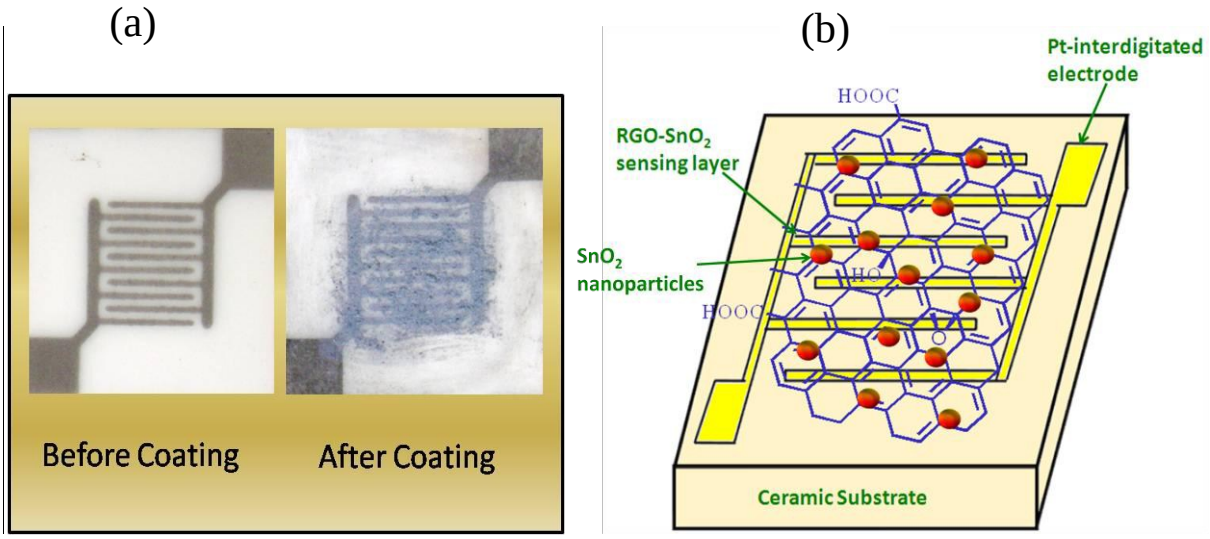

Fig. 6 (a) Photograph of Pt-based interdigitated electrode before and after coating RGO–SnO_2 sensing layer (b) Schematic (not to scale) of RGO−SnO_2 coated Pt-based interdigitated electrodes on ceramic substrate

The samples coated on IDEs were probed inside the stainless steel chamber and purged with dry air for 20 minutes to stabilize the baseline resistances of the samples at room temperature. After that the target gas, here ammonia in presence of 20% relative humidity (RH) was allowed into the chamber for 5 minutes followed by dry air purging. The response of all the samples was calculated as:

$$\text{Response} = \frac{R_{air}}{R_{ammonia}}$$

The response of thermally reduced GO towards ammonia at room temperature is shown in Fig. 7 (a). The resistance of RGO sensor increased when exposed to ammonia as RGO is inherently a p-type material and ammonia is a donor molecule as already been discussed in our previously reported work.[17] SnO_2 is a semiconducting material which senses analytes at higher temperature. So, SnO_2 nanoparticle based sensor was exposed to 1200 ppm ammonia at different temperatures

(150–300ºC) to find out the temperature of its optimum response. The temperature profile and the response of the SnO_2 based sensor towards different concentration of ammonia at its optimum temperature (200°C) are shown in Fig. 7 (b) and 7 (c), respectively.

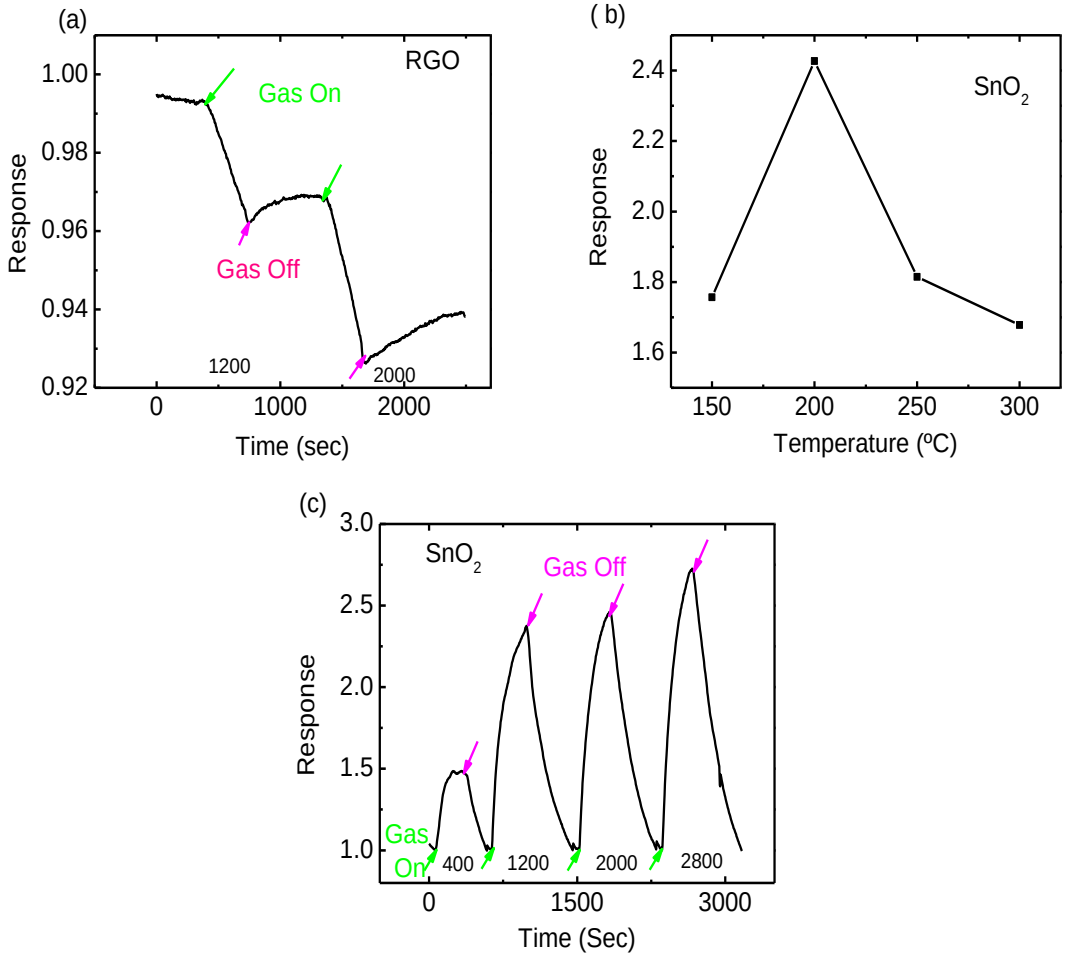

Fig. 7 Response of (a) Thermally reduced GO towards 1200 and 2000 ppm ammonia at room temperature (b) SnO_2 sensor towards 1200 ppm ammonia at four different temperatures (150–300ºC) and (c) SnO_2 sensor towards four different concentrations of ammonia at 200ºC

The basic mechanism of sensing by metal oxide (e.g. tin oxide) has already been discussed in literature.[18] Briefly, when air comes in contact with metal oxide, oxygen molecules trap electrons from the metal oxide surface thereby increasing the sensing layer resistance. These adsorbed oxygen species act as reaction sites when gas molecules (e.g. here NH_3) come in contact with them and thus releasing electrons back to the conduction band of tin oxide.

$$4NH_3 + 3O_{2\,(ads)}^{-} \rightarrow 2N_2 + 6H_2O + 3e^{-}$$

Hence, the resistance of SnO_2 nanoparticle based sensor decreased when exposed to ammonia as can be seen in Fig. 7 (c), thereby depicting n-type behavior of SnO_2 nanoparticle based sensor. The response was found to be 2.4 times in presence of 1200 ppm NH_3 which is much larger than what we got from RGO sensors, but the temperature of sensing was higher than room temperature i.e. 200ºC.

In order to integrate the higher sensitivity of SnO_2 based sensor and the ability of RGO to detect gases at room temperature (which helps in lowering the power dissipation), RGO–SnO_2 hybrid sensing layers were prepared by mixing GO and SnO_2 in different wt%. The sample prepared after mixing GO to SnO_2 in the ratio of 10:3 and then thermally reducing it, demonstrated enhanced sensitivity and that too at room temperature, but the resistance of the hybrid sensing layer increased when exposed to ammonia, thus showing an effective p-type behavior. The response of the hybrid sensor towards four different concentration of ammonia is shown in Fig. 8 (a). The 10:3 (RGO: SnO_2) exhibited a response of 0.665 times against 1200 ppm of ammonia. Again, when the amount of SnO_2 was increased to 10:4 wt% (RGO: SnO_2), the resistance of the hybrid sensor was found to decrease at room temperature when ammonia was introduced to the

test chamber, thus showing an effective n-type behavior. A response of around 3.4 times was observed against 1200 ppm ammonia for the 10:4 (RGO: SnO_2) sample as shown in Fig. 8 (b).

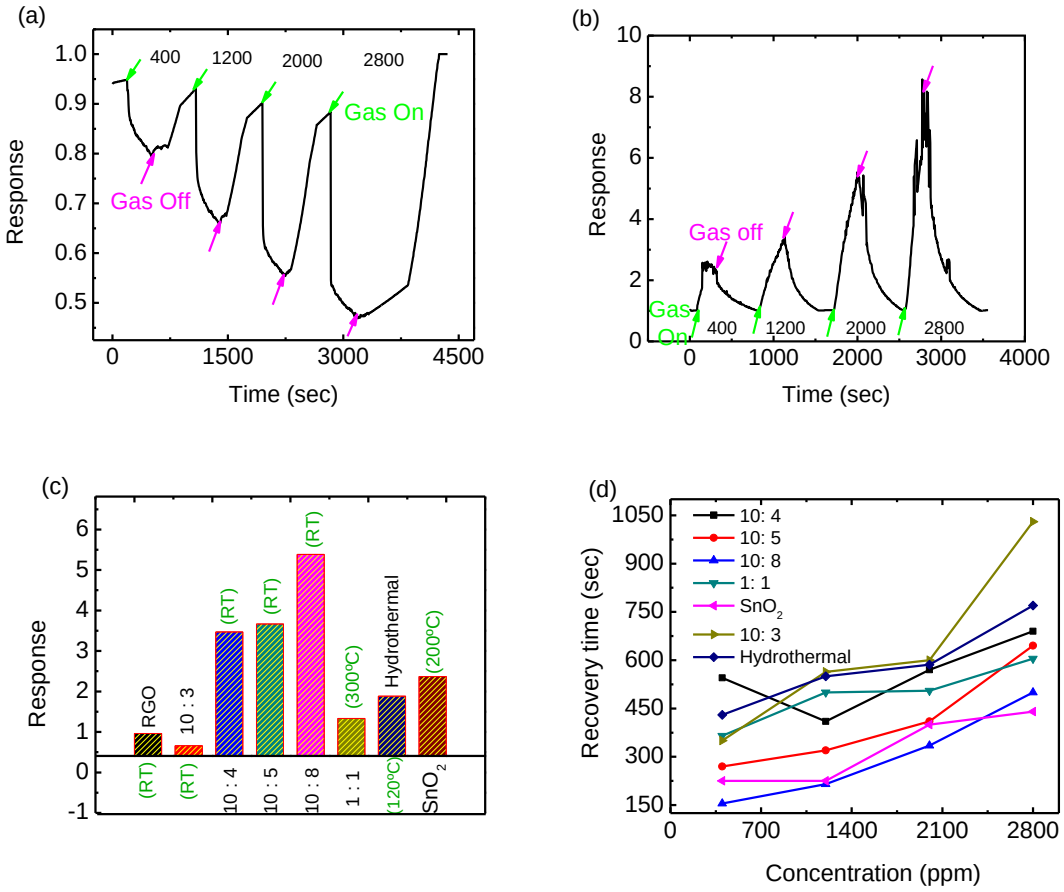

Fig. 8 Response of (a) 10:3 (RGO: SnO_2) (b) 10:4 (RGO: SnO_2) towards four different concentrations of ammonia (400–1200 ppm) (c) comparative response of intrinsic RGO, SnO_2 and RGO–SnO_2 hybrid sensor prepared hydrothermally and by varying the wt% of GO and SnO_2 nanoparticles towards 1200 ppm ammonia (here RT refers to room temperature) and (d) comparative plot of recovery times of intrinsic RGO, SnO_2 and hybrid RGO–SnO_2 sensors

In order to further investigate the role of amount of SnO_2 in the hybrid film, the wt% of SnO_2 was gradually increased and ammonia tests were carried out. It was observed that with increase in amount of SnO_2 in the RGO–SnO_2 hybrid film, the response of the sensors got enhanced

towards ammonia (at room temperature). But when RGO and SnO_2 were mixed in 1:1 ratio, the samples didn't show any measurable resistance up to 290ºC. Such increment of resistance of RGO–SnO_2 hybrid sample is associated with depletion of electrons due to the formation of p−n junction in the hybrid sample as is reported in literature.[19] So, the ammonia test was carried out at 300ºC for this 1:1 ratio sample, but the response was observed to get reduced. For example, the response of this sample towards 1200 ppm ammonia was found to be ~1.3 times only. This response from 1:1 (RGO: SnO_2) ratio sample was found similar to the response of pristine SnO_2 nanoparticle at 300ºC as shown in Fig. 7 (b). This suggests that SnO_2 nanoparticles were playing the predominant role for ammonia sensing in the hybrid samples.

The hydrothermally synthesized hybrid sample also didn't show any measurable resistance at room temperature. This could be explained as follows– RGO can sense gases at room temperature due to its planar 2-D structure. But when the hybrid sample was synthesized hydrothermally, the RGO flakes got folded and formed multilayered structure as is evident in Fig. 3 (d), due to which the 2-D structure no longer existed and thus no resistance could be measured at room temperature. So, the ammonia test was carried out at 120ºC. Also, the response of the hydrothermally synthesized sample was found to be poorer than the samples prepared by mixing GO and SnO_2. As for example, the response of the hydrothermally synthesized sample towards 1200 ppm ammonia was found to be ~1.9 times. The 10:8 (RGO: SnO_2) hybrid sample showed the maximum response towards (measurements carried out at 1200 ppm) ammonia as can be seen in Fig. 8 (c). Also, it was observed that the sensors recovered faster with increase in amount of SnO_2 nanoparticles in hybrid samples as shown in Fig. 8 (d). The recovery time of the 10:8 (RGO: SnO_2) hybrid sensor was found to be shortest among all the sensors. The recovery times of RGO based ammonia sensor was not included in Fig. 8 (d) because the recovery time is

comparatively longer as is evident from the response plot of RGO in Fig 7 (a). The response times of the RGO−SnO_2 hybrid samples were found to be comparable with that of intrinsic SnO_2 nanoparticles but were found very much faster than that of intrinsic RGO. For example, the response time of 10:8 (RGO:SnO_2) sample was found to be around 210 sec against 1200 ppm ammonia whereas the response times of RGO and SnO_2 nanoparticles against 1200 ppm ammonia were 450 and 210 sec respectively. A comparative plot of response times of RGO, SnO_2 hybrid samples for different concentrations of ammonia is shown in Fig. S2 of support information. The response of best sample (10:8 (RGO: SnO_2)) to different concentrations of ammonia is shown in Fig. 9.

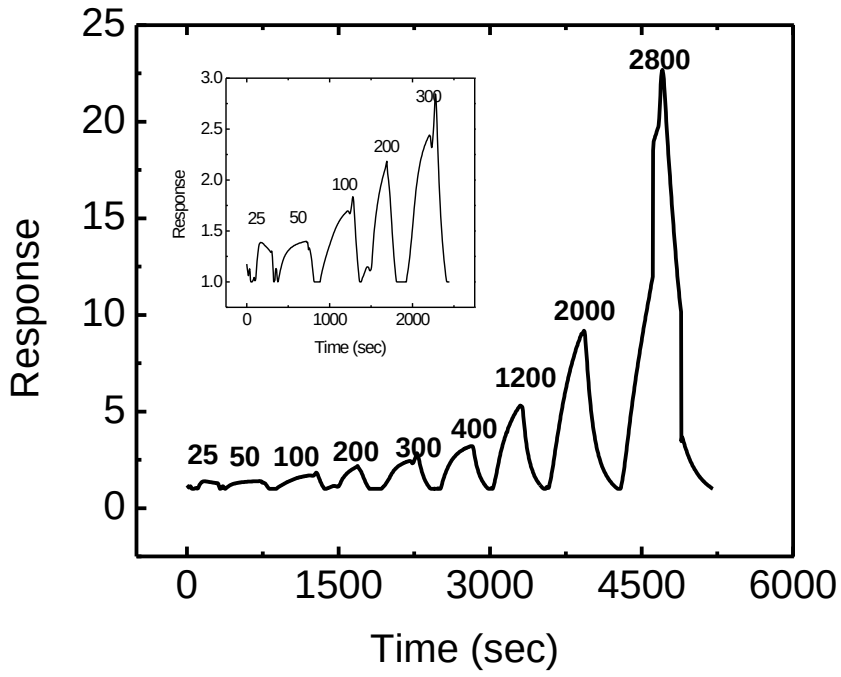

Fig. 9 Response of 10:8 (RGO: SnO_2) sensor towards nine different concentrations of ammonia (25–2800 ppm), inset shows the zoomed in response of the sensor against lower concentration of ammonia (25–300 ppm)

The 10:8 (RGO: SnO_2) sensor was also exposed to nine different concentrations of ammonia (25−2800 ppm) in presence of 20% RH, in order to ensure its performance as practical ammonia sensor. The response of the 10:8 (RGO: SnO_2) sensor was found to be excellent as is shown in Fig. 9 and varied from 1.4 times against 25 ppm ammonia to 22 times against 2800 ppm ammonia. Also, the recovery of the sensor was very fast. It took merely 150 seconds to recover to its baseline resistance after exposure to 400 ppm of ammonia (but in case of RGO the recovery was found to be more than 650 sec which is very slow). The response of all the other hybrid samples against different concentrations of ammonia is shown in support information (Fig. S3, S4, S5). The responses of the sensors are also highly reproducible and repeatable. The reproducible response of our best sample is shown in Fig. 10 (a).

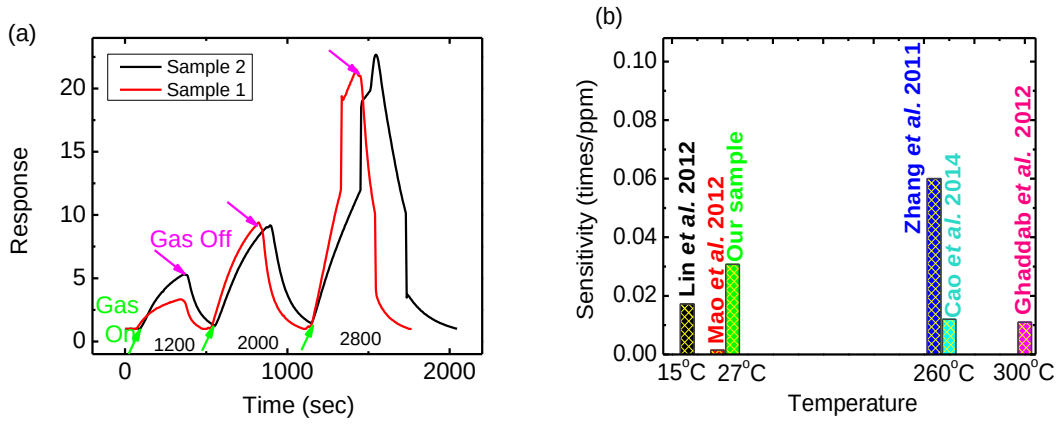

Fig. 10 (a) Reproducible response of 10:8 (RGO: SnO_2) hybrid sensor towards three different concentrations of ammonia (1200–2800 ppm) (b) comparison between the results recently reported on RGO–SnO_2 based ammonia sensor and our samples.

The 10:8 (RGO: SnO_2) hybrid sensor device was prepared twice and the response of both the sensors towards ammonia was found to be almost similar as is shown in Fig. 10 (a). But it was

observed that the recovery of the first sample (Sample 1) was faster than the second sample (Sample 2). The reason is not yet known and needs further investigation.

Recent reports on RGO−SnO_2 based hybrid gas and volatile organic compound (VOC) sensors are available in literature.[20-23] However, in most of the cases the detection temperature was high. A comparison of our achieved response with recently reported literature on RGO–SnO_2 based ammonia sensor is shown in Fig. 10 (b) (only the work reported by Ghaddab *et al.* is on ammonia sensing by SWNT/SnO_2 hybrid).[24-28] The temperature of sensing of all the reported works have been indicated in the plot itself. For our results, the temperature of sensing is room temperature. It was found that our response is better than reported literature against respective concentrations of ammonia. Only the response of the sensors reported by Zhang *et al.* was better than our result, but their working temperature was very high (260ºC). The response of the hybrid ammonia sensor in air ambience reported by Lin *et al.* was found to be poorer than the response (in N_2 ambience) that has been plotted in Fig. 10 (b). They got a response of around 7% i.e. 0.9347 times against 50 ppm of ammonia in air ambience while in our case all the tests were done on air ambience only.

Metal oxide based sensors are supposed to have very poor selectivity. So, in order to ensure the selectivity of our sensor, the 10:8 (RGO: SnO_2) hybrid film was exposed to 1000 ppm of different volatile organic compounds (VOCs) and also to 30% RH.

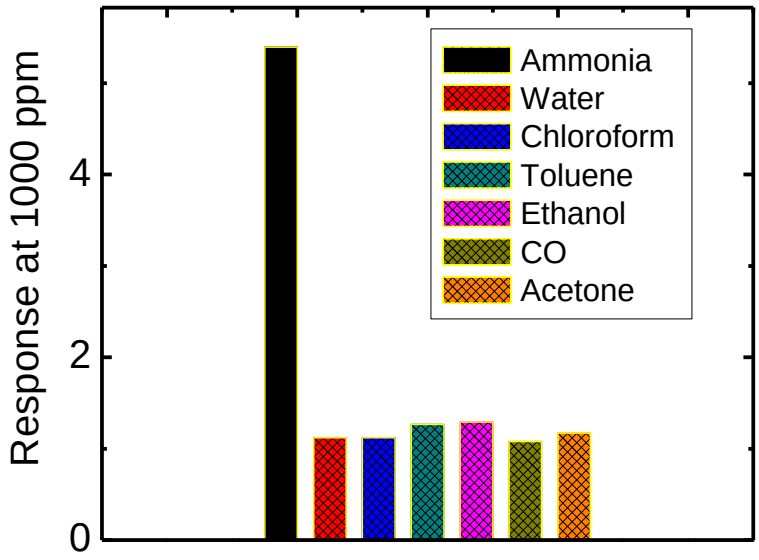

Fig. 11 Comparative response of all the VOCs at 1000 ppm and 30 % RH

The response of the 10:8 (RGO: SnO_2) hybrid sensor towards 1000 ppm of different VOCs were found to be poorer (~1.25 times) than that of 1000 ppm of ammonia (5.6 times) as is evident from Fig. 11. Also, as the ammonia tests were carried out at 20% RH, so, the sensor was also exposed to 30% RH to ensure that there was no considerable contribution of RH to the response of the sensors towards ammonia. And it was observed that the sensor didn't respond well against 30% RH. A mere response of 1.08 times was observed against RH. Hence, the hybrid sensor was found highly selective towards ammonia.

3.2 Sensing mechanism

The basic sensing mechanisms of RGO (predominantly p type due to abundant of holes) and tin oxide (adsorbed oxygen species from air act as reaction sites at the metal oxide surface) are already discussed in the earlier section. However, the hybrid samples exhibited enhanced

response towards ammonia than that of intrinsic RGO and SnO_2. This is because of the formation of hetero and homo junctions at the interface of the materials, (i) RGO-SnO_2 (ii) SnO_2-SnO_2 as is shown in Fig. 12. In case of hetero junction (p-type RGO and n-type SnO_2), SnO_2 donates electrons to RGO which recombine with the holes of RGO thereby shifting the Fermi level and thus a depletion region forms. This depletion region is an additional site for the target gases and attracts electrons from the donor molecules (here ammonia) and results in increase in conductivity. Along with the RGO−SnO_2 depletion zone, SnO_2−SnO_2 depletion region and also the functional groups attached with RGO are active sites for the analytes to react and get attached.

In addition to superior response, our sensors also showed both p-type and n-type behavior, so the sensing mechanism was dominated by the material proportion present in the hybrid film. For example, the 10:3 (RGO: SnO_2) sample demonstrated a p-type behavior towards ammonia which is similar to that shown by intrinsic RGO, but an enhanced response was observed in the hybrid sample. This means the sensing was dominated by RGO being available in abundance, but the enhancement of response was observed due to the presence of SnO_2 nanoparticles which gives rise to different potential barriers at the multiple junctions as mentioned above. The sensing mechanism of the 10:3(RGO: SnO_2) sample is shown in Fig. 12 (a).

On the other hand, the sensing phenomenon of 10:8 (RGO: SnO_2) sample is different than that of 10:3 (RGO: SnO_2) hybrid sample. Here RGO, acted primarily as a conducting network which resulted in a measurable conductivity of the hybrid sample at room temperature even though there is large proportion of tin oxide particle, as is also evident from FESEM image. Here the response of the hybrid sample is predominantly due to the SnO_2−SnO_2 depletion region and the oxide sites presence at the surface of the tin oxide particles as can be seen in Fig. 12 (b). This is

also evident from the effective n-type behavior of the hybrid sensing layer. Also, there is contribution of potential barrier presence at RGO−SnO_2 hetero junction. Thus the response of the hybrid sample for ammonia was found to be much higher than that observed in intrinsic SnO_2 nanoparticles and RGO.

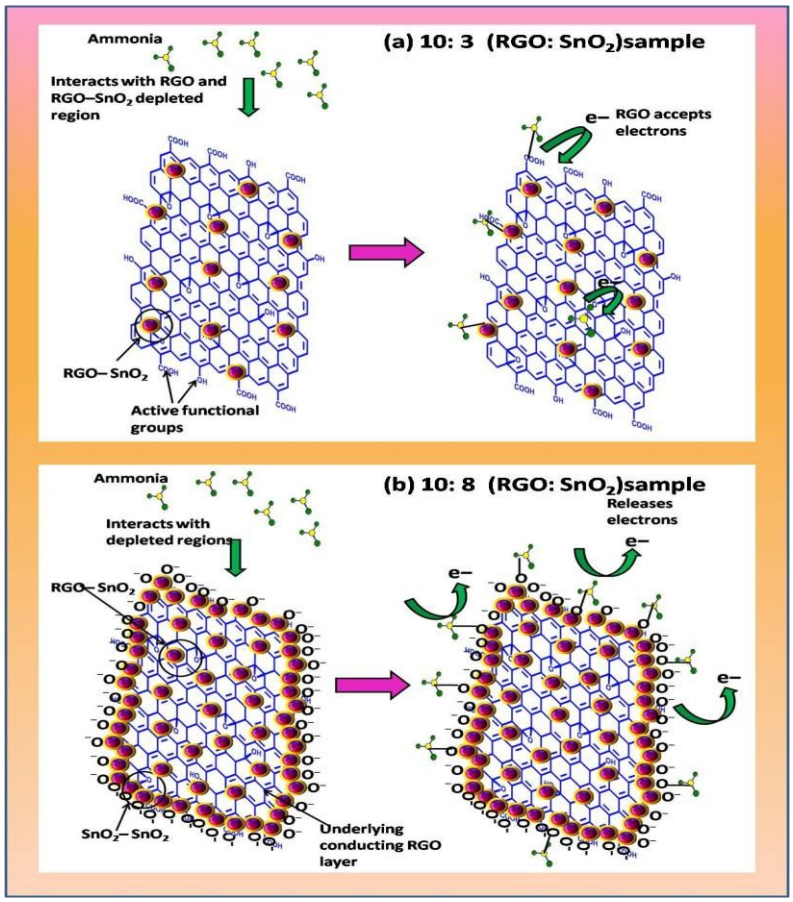

Fig. 12 Schematic (not to scale) representation of sensing mechanism in (a) 10:3 (RGO: SnO_2) sample showing p-type behavior (b) 10:8 (RGO: SnO_2) sample showing n-type behavior

The sensing phenomena of all the n-type behaving samples (10:4, 10:5, 1:1 and hydrothermal) are similar to that of 10:8 samples as explained above. The increase in sensitivity towards ammonia with amount of SnO_2 is due to increase in SnO_2−SnO_2 homojunctions in the sensing layers.

Conclusions

RGO−SnO_2 hybrid ammonia sensors were fabricated. The sensing layers were synthesized by varying the concentration of SnO_2 in RGO and their performances as ammonia detectors at room temperature were observed. Not only an enhanced response over intrinsic RGO and SnO_2 was achieved, but also the sensors recovered faster with high selectivity towards ammonia. The sensing performance of in situ hydrothermally synthesized RGO−SnO_2 hybrid sample was found to be poorer than that of the samples prepared by mixing SnO_2 nanoparticles and RGO (synthesized separately). Also, the hybrid sensor could sense analytes at room temperature, thereby reducing the power consumption of the sensors.

Acknowledgements

S. Santra acknowledges Department of Science and Technology (DST), India for supporting the work partially (project no SR/S2/RJN-104/2011). D. Pradhan and P. K. Guha acknowledge SRIC, IIT Kharagpur for the ISIRD grant to partially support this work. The authors acknowledge DST-FIST Lab (in Department of Physics, IIT Kharagpur) and Central Research Facility, IIT Kharagpur to let us use the XPS facility and FESEM, HRTEM and XRD respectively.

References

1. W. O. B. Timmer, A. van den Berg, *Sensors and Actuators B: Chemical*, 2005, 107, 666–677.
2. M. A. M. Smeets, P. J. Bulsing, S. van Rooden, R. Steinmann, J. A. de Ru, N. W. M. Ogink, C. van Thriel and P. H. Dalton, *Chemical Senses*, 2007, 32, 11-20.

3. K. B. Z. Y. Zhou, J.D. Grunwaldt, T. Fox, L.L. Gu, X.L. Mo, G.R. Chen, G.R. Patzke, *Journal of Physical Chemistry C*, 2011, 115, 1134–1142.

4. W. Tan, Q. Yu, X. Ruan and X. Huang, *Sensors and Actuators B: Chemical*, 2015, 212, 47-54.

5. H. Wang, Y. Qu, H. Chen, Z. Lin and K. Dai, *Sensors and Actuators B: Chemical*, 2014, 201, 153-159.

6. N. D. Chinh, N. Van Toan, V. Van Quang, N. Van Duy, N. D. Hoa and N. Van Hieu, *Sensors and Actuators B: Chemical*, 2014, 201, 7-12.

7. C. A. Betty, S. Choudhury and K. G. Girija, *Sensors and Actuators B: Chemical*, 2014, 193, 484-491.

8. D. K. N. Barsan, U. Weimar, *Sensors and Actuators B: Chemical*, 2007, 121, 18–35.

9. C. Pijolat, B. Riviere, M. Kamionka, J. P. Viricelle and P. Breuil, *Journal of Materials Science*, 2003, 38, 4333-4346.

10. A. K. G. F. Schedin, S. V. Morozov, E. W. Hill, P. Blake, M. I. Katsnelson, K. S. Novoselov, *Nature Materials*, 2007, 6, 652–655.

11. N. Krane, *Selected topics in physics: physics of nanoscale carbon*, 2011.

12. K. S. N. A. K. Geim, *Nature Materials*, 2007, 6, 183-191.

13. S. P. G. Lu, K. Yu, R. S. Ruoff, L. E. Ocola, D. Rosenmann, J. Chen, *ACS Nano*, 2011, 5, 1154–1164.

14. A. M. Ruma Ghosh, Sumita Santra, Samit K. Ray, and Prasanta K. Guha, *ACS Applied Materials and Interfaces*, 2013, 5, 7599−7603.

15. S. Bazargan, N. F. Heinig, D. Pradhan and K. T. Leung, *Crystal Growth & Design*, 2011, 11, 247-255.

16. X. Gao and X. Tang, *Carbon*, 2014, 76, 133-140.

17. A. S. Ruma Ghosh, Sumita Santra, Samit K. Ray, Amreesh Chandra,Prasanta K. Guha, *Sensors and Actuators B: Chemical*, 2014, 205, 67–73.

18. K. Wetchakun, T. Samerjai, N. Tamaekong, C. Liewhiran, C. Siriwong, V. Kruefu, A. Wisitsoraat, A. Tuantranont and S. Phanichphant, *Sensors and Actuators B: Chemical*, 2011, 160, 580-591.

19. H. Zhang, J. Feng, T. Fei, S. Liu and T. Zhang, *Sensors and Actuators B: Chemical*, 2014, 190, 472-478.

20. G. Neri, S. G. Leonardi, M. Latino, N. Donato, S. Baek, D. E. Conte, P. A. Russo and N. Pinna, *Sensors and Actuators B: Chemical*, 2013, 179, 61-68.

21. D. C. Li Yin, Xue Cui, Lianfang Ge, Jing Yang, Lanlan Yu, Bing Zhang, Rui Zhang, and Guosheng Shao, *Nanoscale*, 2014, 6, 13690–13700.

22. B. H. J. S. J. Choi, S. J. Lee, B. K. Min, A. Rothschild, and D. Kim, *ACS Applied Materials & Interfaces*, 2014, 6, 2588−2597.

23. D. Zhang, A. Liu, H. Chang and B. Xia, *RSC Advances*, 2015, 5, 3016-3022.

24. J. B. S. B. Ghaddab, C. Mavon, M. Paillet , R. Parret, A.A. Zahab, J.-L. Bantignies,V. Flaud, E. Beche, F. Berger, *Sensors and Actuators B: Chemical*, 2012, 170, 67–74.

25. R. Z. Zhenyu Zhang, Guosheng Song, Li Yu, Zhigang Chen and Junqing Hu, *Journal of Material Chemistry C*, 2011, 21, 17360–17365.

26. Y. L. Qianqian Lin, Mujie Yang, *Sensors and Actuators B: Chemical*, 2012, 173, 139–146.

27. S. C. Shun Mao, Ganhua Lu, Kehan Yu, Zhenhai Wen and Junhong Chen, *Journal of Material Chemistry C*, 2012, 22, 11009–11013.

28. Y. L. Yali Cao, Dianzeng Jia and Jing Xie, *RSC Advances*, 2014, 4, 46179–46186.